JOURNAL OF CATALYSIS 84, 119–134 (1983)

Deactivation of Nickel Methanation Catalysts Induced by the Decomposition of Iron Carbonyl

I. Deactivation via Pore-Mouth Blocking

WEI-MING SHEN,[1] JAMES A. DUMESIC,[2] AND CHARLES G. HILL, JR.

Department of Chemical Engineering, University of Wisconsin, Madison, Wisconsin 53706

Received February 1, 1983; revised April 12, 1983

The deactivation of alumina-supported nickel methanation catalysts due to decomposition of $Fe(CO)_5$ was studied using both reaction kinetics measurements and *in situ* Mössbauer spectroscopy. Iron carbonyl, enriched in ^{57}Fe for Mössbauer spectroscopy studies, was produced *in situ* and entrained with the carbon monoxide feed to a methanation reactor operating at temperatures of 620–650 K and H_2/CO ratios near 7. This incorporation of Fe into the nickel catalyst via the decomposition of $Fe(CO)_5$ resulted in significant catalyst deactivation as well as changes in the parameters of a power law rate expression describing the methanation kinetics. With increasing amounts of Fe deposited on the catalyst, the kinetic parameters were shifted toward those of iron catalysts. These iron-induced phenomena are due to (1) pore-mouth blocking of the Al_2O_3 micropore structure by iron particles formed during the diffusion-limited decomposition of $Fe(CO)_5$, and (2) interactions between iron and nickel in the macropores of the support. Specifically, the loss of catalyst activity is primarily caused by pore-mouth blocking, while shifts in kinetic parameters are the consequence of both pore-mouth blocking and interactions between iron and nickel. The majority of the iron deposited under methanation reaction conditions has been identified as χ-carbide (Hägg carbide) using Mössbauer spectroscopy at liquid helium temperature.

INTRODUCTION

Deactivation of nickel methanation catalysts is most often due to growth of nickel particles, sulfur poisoning, and carbon deposition. Typical methanation reactors are operated at pressures of 1–3 MPa and inlet temperatures of 530–670 K (*1–4*). Studies on the thermal stability of supported Ni catalysts (*5–7*) suggest that at these temperatures sintering of Ni does not take place in He, N_2, or H_2. However, operation of nickel methanation catalysts under conditions of low temperatures and high CO partial pressures can result in growth of nickel particle size via the formation of $Ni(CO)_4$ (*8*). Deactivation by sulfur poisoning is believed to proceed via blockage of surface sites by sulfur atoms strongly adsorbed on the Ni surface (*9–12*). Although published data (*13–15*) indicate the absence of massive carbon deposition on Ni catalysts under methanation conditions, blockage of active sites by surface carbon deposits may take place (*16, 17*). The nature of these inactive carbon deposits is believed to be graphitic (*18–20*). Details of this deactivation mode have been discussed in recently published review articles (*21, 22*).

In addition to the above mentioned deactivation mechanisms, there is another less-known "poison" which can cause the deactivation of nickel methanation catalysts, i.e., $Fe(CO)_5$ formed in the coal gasification process. A coal gasifier is typically operated at pressures of 2.4–3.2 MPa and outlet temperatures of 680–930 K (*23*). The outlet

[1] Present address: Union Carbide Corporation, Parma Technical Center, P.O. Box 6116, Cleveland, Ohio 44101.

[2] To whom all correspondence should be addressed.

0021-9517/83 $3.00

gas contains a high concentration of CO (10–60%) (*2, 23*). This CO can react with the carbon steel piping used for gas transmission to form volatile iron carbonyls. This entrained iron carbonyl can later decompose in the methanation catalyst bed causing deactivation of the nickel catalyst. It has been reported that an iron concentration of 0.18 mg/m^3 (equivalent to 70 ppb) was found in the recycle stream of a pilot plant operation (*24*) in which deactivation of a Raney nickel catalyst was observed. In contrast to the other deactivation mechanisms, there are no published studies aimed at unveiling the mechanism of catalyst deactivation due to decomposition of iron carbonyl. Thus, the objective of the present study was to elucidate the mechanism of this mode of catalyst deactivation. Kinetics measurements, *in situ* Mössbauer spectroscopy, and Auger electron spectroscopy were used in this respect.

In short, it was observed in this study that incorporation of iron into alumina-supported nickel catalysts via the decomposition of iron carbonyl caused decreases in catalyst activity as well as changes in the kinetic parameters of the methanation reaction. These results are discussed in terms of (i) blockage of the mouths of the micropores of the Al_2O_3 support by Fe particles formed as a result of diffusion-limited decomposition of iron carbonyl, and (ii) interactions between the nickel particles in the macropores and the iron deposited on these particles. This paper reports experimental results dealing with the phenomenon of pore-mouth blocking. Also included is a discussion of the Mössbauer spectroscopy studies carried out to identify the iron carbide phase formed under methanation reaction conditions. The results confirming Fe–Ni interactions will be published in a later paper (*25*).

EXPERIMENTAL

In Situ Production of Fe(CO)$_5$

To simulate the conditions under which Fe(CO)$_5$-induced deactivation of a Ni methanation catalyst occurs (*24*), low concentrations of ^{57}Fe(CO)$_5$ were produced *in situ* for use within the high pressure reaction system described elsewhere (*8*). The use of ^{57}Fe-enriched iron carbonyl is essential for collecting *in situ* Mössbauer spectra at low concentrations of Fe. The *in situ* production of Fe(CO)$_5$ was accomplished by reacting high pressure CO with iron supported on alumina in a "carbonyl reactor." Located in the carbon monoxide feed line upstream of the high pressure methanation reactor, this "carbonyl reactor" was made of a piece of 316 stainless-steel tubing, operated at P_{CO} = 4.0 MPa and T = 473 K. After passing through this reactor, the CO containing entrained Fe(CO)$_5$ was then mixed with H_2 to produce synthesis gas of the desired composition. The Fe(CO)$_5$ was then carried in the synthesis gas stream, and subsequently decomposed on the methanation catalyst at 620–650 K.

The supported iron catalysts used in the "carbonyl reactor" (9.8 wt% Fe on α-Al_2O_3) were prepared by multiple incipient wetness impregnation using 80/200 mesh low surface area α-Al_2O_3 and aqueous $Fe(NO_3)_3$ solution. To synthesize a catalyst containing Fe with its natural abundance of ^{57}Fe, $Fe(NO_3)_3 \cdot 9H_2O$ (Baker analyzed reagent) was used for preparation of the impregnation solution. The impregnation solution for synthesizing an ^{57}Fe-enriched catalyst was prepared by first reducing ^{57}Fe-enriched Fe_2O_3 powder (Oak Ridge National Lab, enriched to 86 atomic% in ^{57}Fe) in flowing H_2 at 723 K for 24 h, then dissolving the reduced iron in 30 wt% HNO_3 (at room temperature) without exposure to air. The iron catalysts were dried at 388 K for at least 2 h after each impregnation. Once the desired metal loading was reached, the sample was then (i) dried overnight at 388 K, (ii) reduced in flowing H_2 at 723 K for 24 h, and (iii) passivated by air (at room temperature) which was allowed to diffuse into the He-filled reduction cell. Approximately 0.5 g of this passivated catalyst was loaded into the "carbonyl reactor."

Catalyst Preparation

The 5.74 wt% $Ni/\gamma\text{-}Al_2O_3$ catalyst used in these experiments was prepared by incipient wetness impregnation using Davison SMR-7 $\gamma\text{-}Al_2O_3$ powder (170/200 mesh) and aqueous $Ni(NO_3)_2$ solution. After 2.5 h of hydrogen reduction treatment at 723 K (*8*), the catalyst was loaded into a quartz cell and sintered by heating in flowing hydrogen at 1070 K for 14 h. This pretreatment prevented the reaction from igniting in studies of kinetics at high temperatures (ca. 620 K). The range of carbon monoxide partial pressures used in this study required the use of high reaction temperatures to avoid rapid deactivation of the Ni catalyst (*8*). The sintered catalyst (ca. 0.25 g) was then loaded into the high pressure Mössbauer spectroscopy cell described elsewhere (*26*). It was reduced for 2.5 h at 723 K in flowing hydrogen prior to the methanation kinetics studies.

Chemical analyses of catalyst samples were carried out by Galbraith Laboratories, Inc.

Methanation Kinetics

The kinetics of the methanation reaction were studied in the 316 stainless-steel high pressure reaction system described elsewhere (*8*). Space velocities of ca. 2×10^5 $cm^3 \cdot g^{-1} \cdot h^{-1}$ (based on the reactor inlet conditions) were used to keep CO conversions low at the high reaction temperatures employed. This approach permitted the data to be analyzed using a differential reactor model.

The decrease in methanation activity of the Ni catalyst was monitored during exposure of the catalyst to a given CO/H_2 gas mixture containing $Fe(CO)_5$. The "carbonyl reactor" was then bypassed, and the deactivated catalyst was treated in flowing H_2 until no CH_4 could be observed in the effluent gas from the Mössbauer spectroscopy cell (ca. 2.5 h). The methanation kinetics of this partially deactivated catalyst were then studied, as described elsewhere (*8*). These procedures were repeated for each dose of $Fe(CO)_5$.

Mössbauer Spectroscopy

In situ Mössbauer spectra were obtained using Austin Science Associates electronics and a 1024 channel Tracor Northern TN-1705 multichannel analyzer. The source, 50 mCi of ^{57}Co diffused into a Pd matrix, was supplied by New England Nuclear. The Doppler velocity was calibrated with a 12.7-μm metallic iron foil. Isomer shifts are reported relative to this standard absorber at room temperature. Mössbauer spectra were fitted using a computer program described elsewhere (*27*).

After each dose of $Fe(CO)_5$, *in situ* Mössbauer spectra of the partially deactivated nickel catalyst were collected either under methanation reaction conditions or at room temperature in flowing H_2. The catalyst was quenched either in flowing H_2 after hydrogen regeneration treatments or in flowing H_2 with decreasing amounts of CO following methanation kinetics studies. In the latter case, the catalyst was not cooled in flowing H_2/CO reactant mixtures typical of methanation conditions (e.g., 10% CO) in order to avoid possible formation of $Ni(CO)_4$ at lower temperatures (*8*). It took 5 min to cool the catalyst from ca. 633 to 450 K, and 10 min to cool to ca. 380 K.

To obtain a better signal-to-noise ratio, the Mössbauer data registered in every two consecutive channels in the multichannel analyzer were added prior to computer fitting. The new set of data thus formed had one-half the number of channels, but twice the number of pulse counts in each channel. This manipulation increased the signal-to-noise ratio at the expense of resolution on the energy scale, and it had essentially no effect on the Mössbauer parameters of the metallic iron standard used for calibration of the spectrometer.

Mössbauer Spectroscopy Study at Liquid Helium Temperature

Low temperature Mössbauer spectra

were obtained on another Mössbauer spectrometer equipped with a 512 channel Tracor Northern NS-900 multichannel analyzer. An $Fe(CO)_5$ deactivated nickel catalyst was first transferred from the high pressure Mössbauer spectroscopy cell to a vacuum tight, Plexiglas sample cell using a He-filled glove bag. The sample cell was then attached to the tip of the cold head of the liquid helium refrigerator operated at 10 K (Air Products and Chemicals, Inc., LT-3-110 Heli-Tran Liquid Helium Transfer Refrigerator). Details of the sample cell and transfer procedure have been described elsewhere (*28*).

RESULTS

Activity and Kinetics of the Methanation Reaction

A blank run was carried out with 0.265 g of 170/200 mesh γ-Al_2O_3 powder in the high pressure Mössbauer spectroscopy cell. There was no detectable methanation activity at reduced space velocities (ca. 1×10^5 $cm^3 \cdot g^{-1} \cdot h^{-1}$) and temperatures as high as 673 K. This observation indicates that neither the alumina powder nor the Mössbauer spectroscopy cell was contributing to the methanation kinetics observed with the Ni catalysts.

The methanation activities of supported Ni catalysts before, during and after the introduction of $^{57}Fe(CO)_5$ are shown in Figs. 1 and 2 as functions of time on-stream for runs NiFe-2 and NiFe-3, respectively. (The "NiFe" in the run numbers indicates that the series of experiments was carried out with an $Fe(CO)_5$-deactivated Ni/Al_2O_3 catalyst.) Similar results were observed for run NiFe-1, where $Fe(CO)_5$ with the natural abundance of ^{57}Fe was used. Before the introduction of $Fe(CO)_5$, the fresh catalysts showed a 15–20% decrease in activity during the initial 5 h. Thereafter, the catalytic activity remained relatively constant, showing only a 15% decrease in activity over a period of 20 h. (All percentages are normalized against the initial catalytic activity measured upon exposure of the catalyst to reaction conditions.) In run NiFe-2,

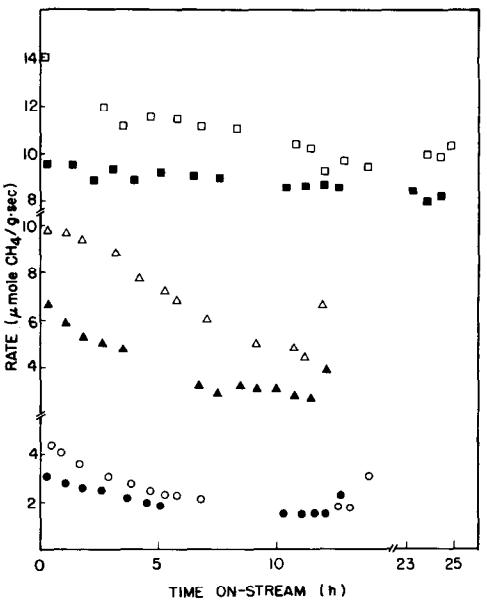

FIG. 1. Deactivation studies of Ni/Al_2O_3 (run NiFe-2) for P_{H_2} = 130 kPa and P_{CO} = 18.6 kPa. □, Fresh catalyst at 613 K. ■, Catalyst at 613 K after the first deactivation study and kinetic studies. △, Catalyst at 623 K during the first exposure to $^{57}Fe(CO)_5$. ▲, Catalyst at 623 K after 11 h exposure to $^{57}Fe(CO)_5$. ○, Catalyst at 633 K during the second exposure to $^{57}Fe(CO)_5$. ●, Catalyst at 633 K after 24 h (cumulative) exposure to $^{57}Fe(CO)_5$. The last point in each series of deactivation studies was collected after H_2 treatment at the respective deactivation temperature for at least 2 h.

the Fe/Al_2O_3 catalyst used for $Fe(CO)_5$ production was not reduced *in situ*. During the first $Fe(CO)_5$ treatment, there was an induction period of ca. 2.5 h, during which the activity of the catalyst decreased only slightly (Fig. 1). The catalytic activity then dropped sharply by 50% within 8 h. No induction period was observed during the second exposure of the catalyst to $Fe(CO)_5$. In particular, the catalyst showed an initial sharp decrease in activity by 50% within 8 h; activity was constant thereafter. In run NiFe-3, the Fe/Al_2O_3 catalyst was regenerated in flowing H_2 prior to each dose of $Fe(CO)_5$. Upon exposure to synthesis gas containing entrained $Fe(CO)_5$, the nickel catalyst rapidly lost methanation activity (Fig. 2). Hence, the induction period observed in the first $Fe(CO)_5$ treatment of run NiFe-2 is attributed to the presence of a

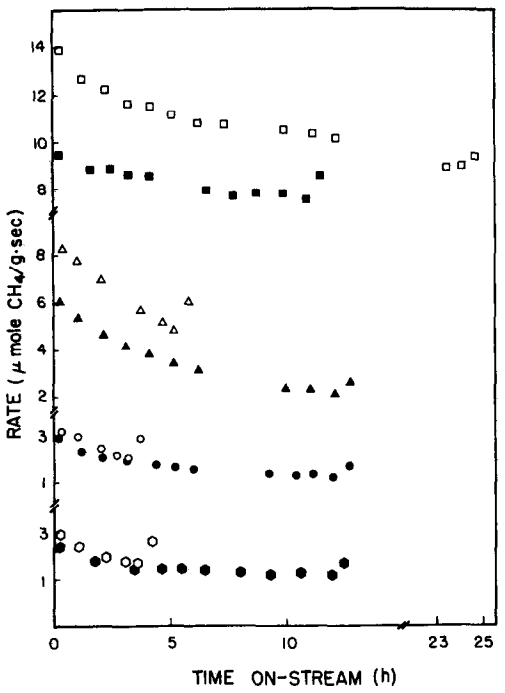

FIG. 2. Deactivation studies of Ni/Al_2O_3 (run NiFe-3) for P_{H_2} = 130 kPa and P_{CO} = 18.1 kPa. □, Fresh catalyst at 613 K. ■, Catalyst at 613 K after the first deactivation study. △, Catalyst at 623 K during the first exposure to $^{57}Fe(CO)_5$. ▲, Catalyst at 623 K after 4.5 h exposure to $^{57}Fe(CO)_5$. ○, Catalyst at 633 K during the second exposure to $^{57}Fe(CO)_5$. ●, Catalyst at 633 K after 7.0 h (cumulative) exposure to $^{57}Fe(CO)_5$. ⬡, Catalyst at 653 K during the third exposure to $^{57}Fe(CO)_5$. ⬢, Catalyst at 648 K after 9.7 h (cumulative) exposure to $^{57}Fe(CO)_5$. The last point in each series of deactivation studies was collected after H_2 treatment at the respective deactivation temperature for at least 2 h. The supported Fe catalyst for *in situ* production of $Fe(CO)_5$ was regenerated in flowing H_2 before each dose of $Fe(CO)_5$.

surface oxide on the Fe/Al_2O_3 catalyst. The treatment in a reducing atmosphere (CO for the second dose of $Fe(CO)_5$ in run NiFe-2 and H_2 prior to the $Fe(CO)_5$ dose in run NiFe-3) eliminates the surface oxide and the induction period associated therewith.

The deactivation studies carried out after completion of each treatment with $Fe(CO)_5$ showed similar results for all sets of experiments. The catalytic activity decreased by ca. 50% in the initial 5 h. This decrease was followed by a more moderate drop in activity. It was also noted that a substantial amount of the lost activity for the iron-containing catalyst could be recovered by H_2 treatment at reaction temperatures (623–653 K). For iron-free catalysts, the recovery of activity after regeneration was minimal after similar treatment in H_2.

In addition to the Fe deposited in the catalyst bed, iron was also deposited on the walls of the Mössbauer spectroscopy cell. The contribution of this iron deposit to the observed methanation activity was experimentally determined to be insignificant. Specifically, its contribution accounted for only 4.3–5.4% of the observed catalyst activity of the deactivated nickel catalyst used in run NiFe-3.

As shown in Figs. 3 and 4, systematic changes were observed when the kinetic parameters characteristic of the methanation reaction over Fe-free catalysts were compared with those of the same catalysts after increasing exposures to $Fe(CO)_5$. The kinetic parameters are summarized in Table 1. Published results (*29*) for methanation over Fe/Al_2O_3 and Ni/Al_2O_3 catalysts are also included in Table 1 for comparison. Increasing the amount of Fe deposited on the Ni catalyst (i) decreases the activation en-

TABLE 1

Summary of Kinetic Parameters[a] for Ni/Al_2O_3 before and after Exposure to $Fe(CO)_5$

	E_A (kJ/mol)	X	Y
Run NiFe-1			
Fresh Ni/Al_2O_3	117	0.65	0.04
22.5 h exposure to $Fe(CO)_5$	112	0.66	0.03
66 h exposure to $Fe(CO)_5$	78	1.05	0.09
Run NiFe-2			
Fresh Ni/Al_2O_3	118	0.65	0.11
11 h exposure to $Fe(CO)_5$	87	0.96	0.06
24 h exposure to $Fe(CO)_5$	78	1.04	0.06
Run NiFe-3[b]			
Fresh Ni/Al_2O_3	120	0.74	0.11
4.5 h exposure to $Fe(CO)_5$	91	0.89	0.06
7.0 h exposure to $Fe(CO)_5$	77	1.04	0.04
9.7 h exposure to $Fe(CO)_5$	70	1.03	0.10
Literature kinetic parameters[c]			
5% Ni/Al_2O_3	105	0.77	−0.31
15% Fe/Al_2O_3	89	1.14	−0.05

[a] $r_{CH_4} = A \exp(-E_A/RT)\, P_{H_2}{}^X P_{CO}{}^Y$.

[b] The supported iron catalyst (for producing $Fe(CO)_5$) was regenerated in flowing H_2 before each dose of $Fe(CO)_5$.

[c] Results of kinetic studies by Vannice (*29*).

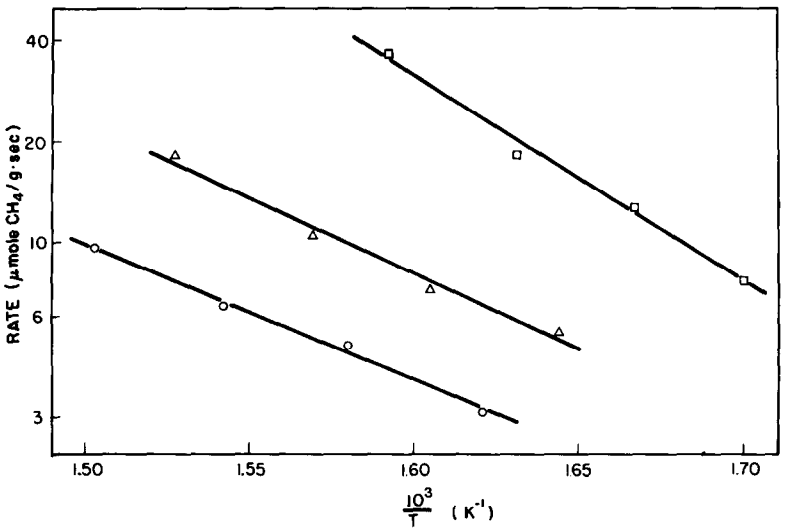

FIG. 3. Arrhenius plots of run NiFe-2 for P_{H_2} = 281 kPa and P_{CO} = 23.4 kPa. □, Fresh Ni/Al_2O_3 catalyst. △, Ni/Al_2O_3 catalyst after 11 h exposure to $^{57}Fe(CO)_5$. ○, Ni/Al_2O_3 catalyst after 24 h exposure to $^{57}Fe(CO)_5$.

ergy, (ii) increases the dependence of the rate on hydrogen partial pressure, and (iii) does not affect the dependence of the rate on CO partial pressure. It was also noted that the methanation rate over an iron-deactivated nickel catalyst appears to become zero-order in hydrogen at high hydrogen partial pressures (ca. 413 kPa) (see Fig. 4).

Catalyst Characterization Using Mössbauer Spectroscopy

Room temperature Mössbauer spectra of the iron-containing nickel methanation catalysts immediately after dosing with $Fe(CO)_5$ and after treatments under methanation reaction conditions are shown in Fig. 5. The major component in these spectra is the broad spectral component due to an iron carbide phase. Although the spectrum becomes partially magnetically split at higher iron concentrations (see spectra (c) and (d)), a positive identification of the iron carbide phase is not possible on the basis of these broad absorption peaks. The sharp absorption doublet near zero Doppler velocity comes mainly from the iron impurity in the beryllium windows on the Mössbauer spectroscopy cell. Its contribution to any Mössbauer spectrum remains constant and can be constrained in computer fits to that determined in spectra of the blank runs (*26*). The third component in these spectra is the contribution from Fe^{2+}. Its presence is manifested by the broad shoulder (in spectra (a) and (b)) and by the broad peak (in spectra (c) and (d)) at +2.0 mm/s (e.g.,

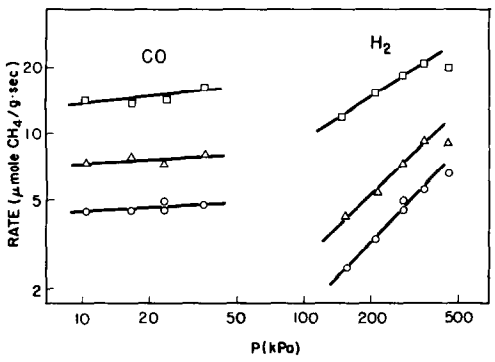

FIG. 4. Partial pressure dependence of methanation rate from run NiFe-2. Hydrogen partial pressure was kept at 283 kPa for CO partial pressure dependence studies, while P_{CO} = 23.4 kPa for H_2 partial pressure dependence studies. □, Fresh Ni/Al_2O_3 catalyst at 613 K. △, Ni/Al_2O_3 catalyst at 623 K after 11 h exposure to $^{57}Fe(CO)_5$. ○, Ni/Al_2O_3 catalyst at 633 K after 24 h exposure to $^{57}Fe(CO)_5$.

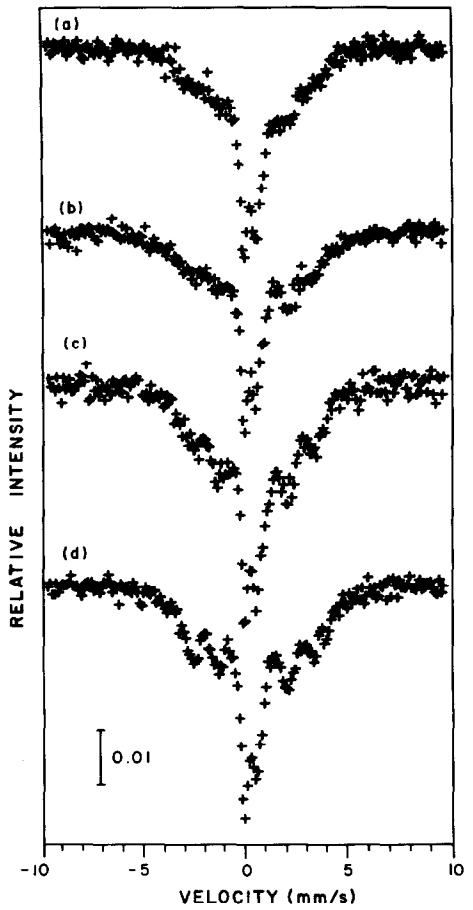

FIG. 5. Mössbauer spectra collected at room temperature in flowing H_2 after quenching the sample from reaction conditions (run NiFe-3). For spectra (a) and (b), the sample had 7.0 h exposure to $^{57}Fe(CO)_5$ in two doses. This sample was given an additional 2.7 h exposure to $^{57}Fe(CO)_5$, before spectra (c) and (d) were collected. Spectrum (a): Immediately after $^{57}Fe(CO)_5$ treatment. Spectrum (b): After 25 min in synthesis gas (H_2:CO = 8:1) at 633 K. Spectrum (c): Immediately after $^{57}Fe(CO)_5$ treatment. Spectrum (d): After 25 min in synthesis gas (H_2:CO = 8:1) at 648 K.

see Ref. (*30*)). The other absorption peak of the Fe^{2+} doublet overlaps with the doublet arising from the iron impurity in the beryllium windows.

Room temperature Mössbauer spectra of the iron-containing nickel methanation catalysts after H_2 treatment are shown in Fig. 6. The solid lines are the results of computer fitting these spectra. The corresponding computer-fitted Mössbauer parameters are summarized in Table 2. The existence of ferromagnetic metallic iron in the catalyst is manifested by the four outer peaks, at approximately ±5 and ±3 mm/s, of a spectral sextuplet. The inner two absorption peaks of the sextuplet are masked by the doublet near zero Doppler velocity. As in the case of the spectra shown in Fig. 5, the iron impurity in the beryllium windows makes a significant contribution to this central doublet. Another component in the catalyst is Fe^{2+}, as evidenced by the broad peak at +2.0 mm/s. However, the spectra cannot be satisfactorily fitted with only the three components mentioned above. A

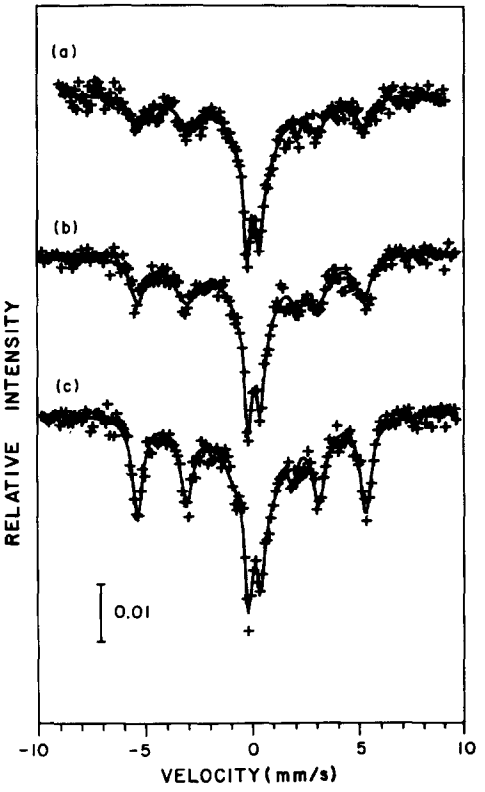

FIG. 6. Room temperature Mössbauer spectra of samples (run NiFe-3) after H_2 treatment. The results of computer fitting are indicated by the solid lines. Spectrum (a): After 4.5 h exposure to $^{57}Fe(CO)_5$ in one dose. Spectrum (b): After 7.0 h exposure to $^{57}Fe(CO)_5$ in two doses. Spectrum (c): After 9.7 h exposure to $^{57}Fe(CO)_5$ in three doses.

TABLE 2

Computer-Fitted Mössbauer Parameters of Spectra Shown in Fig. 6

Fe-containing phases	Spectral area[a] (%)	Mössbauer parameters[b]
Spectrum (a)		
Ferromagnetic metallic iron	56.4	H = 324 kOe QS = −0.021 mm/s IS = 0.051 mm/s
Fe^{2+}	5.8	QS = 2.250 mm/s IS = 1.022 mm/s
Fe^0 (broad singlet)	37.8	IS = 0.299 mm/s
Spectrum (b)		
Ferromagnetic metallic iron	61.8	H = 327 kOe QS = −0.026 mm/s IS = −0.002 mm/s
Fe^{2+}	9.3	QS = 2.232 mm/s IS = 1.002 mm/s
Fe^0 (broad singlet)	28.9	IS = 0.261 mm/s
Spectrum (c)		
Ferromagnetic metallic iron	64.0	H = 332 kOe QS = −0.021 mm/s IS = 0.006 mm/s
Fe^{2+}	6.3	QS = 2.017 mm/s IS = 0.910 mm/s
Fe^0 (broad singlet)	29.7	IS = 0.257 mm/s

[a] Relative spectral areas calculated excluding the contribution from the iron impurity in the Be windows.

[b] H, QS, and IS are magnetic hyperfine field, quadrupole splitting and isomer shift, respectively. All isomer shifts are relative to metallic iron at room temperature.

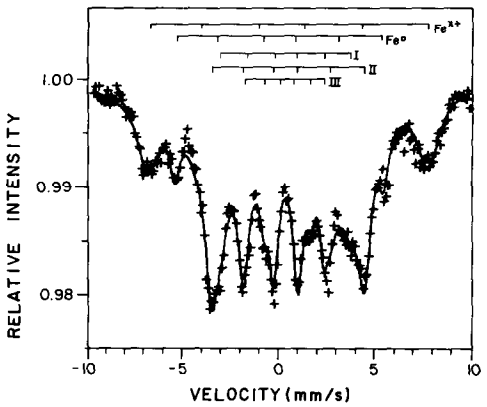

FIG. 7. Mössbauer spectrum collected at 10 K after 9.7 h exposure to $^{57}Fe(CO)_5$ in three doses and quenching from reaction conditions (run NiFe-3). The room temperature spectrum of this sample within the Mössbauer spectroscopy cell is shown as spectrum (d) of Fig. 5. The computer-fitted peak positions are indicated by means of stick diagrams. I, II, and III refer to the three magnetically different sites for iron atoms in the χ-carbide phase. The solid line shows the results of the computer fitting.

fourth component, with a very broad singlet and a slightly positive isomer shift (IS = 0.25–0.30 mm/s, linewidth ca. 2.0 mm/s), is needed for any reasonably good fit of the Mössbauer data. It is denoted as "Fe^0 (broad singlet)" in Table 2. The significance of this singlet will be discussed later. During the initial stages of computer fitting, the positions of the inner two peaks of the ferromagnetic metallic iron sextuplet were constrained to be the same as those determined in the metallic iron calibration spectrum, and the peak widths and dips of these two peaks were required to be comparable to those of the four outer peaks at ±5 and ±3 mm/s. However, these constraints were released when the final fit was made to obtain the results reported in Table 2.

Figure 7 shows the Mössbauer spectrum at 10 K of the catalyst after treatment under methanation reaction conditions. The computer-fitted peak positions are indicated by means of stick diagrams. The solid line shows the results of computer fitting this

TABLE 3

Magnetic Hyperfine Fields of Iron Species in the Mössbauer Spectrum at 10 K of the Sample from Run NiFe-3 (Fig. 7)

Iron species	Relative spectral area (%)	Computer-fitted value (kOe)	Literature value (kOe)	Reference
Iron oxide	25.2	452	544	31
Metallic iron	8.8	338	338	32
Iron carbide[a]				
I	29.4	211	220	33[b]
II	28.4	248	252	33
III	8.2	129	134	33

[a] I, II, and III refer to the three magnetically different sites for iron atoms in the monoclinic structure of χ-carbide.

[b] The assignment of sites I and II by Le Caer *et al.* (*33*) is opposite to that of others (e.g., Unmuth *et al.* (*15*), Raupp and Delgass (*35*)). The latter convention is adopted in the present assignment.

spectrum. (Since this spectrum was collected using the liquid helium refrigerator and a sample cell fabricated from Plexiglas, there were no contributions to the spectrum from the iron impurities in the Be windows as in the case of the *in situ* catalyst spectra.) The following iron phases can be identified from this spectrum: χ-carbide, iron oxide, and metallic iron. The relative spectral areas and magnetic hyperfine fields of these phases are shown in Table 3. It can be seen that χ-carbide is the major iron-containing phase. Due to the complexity of this spectrum, the computer-fitting was begun with the following constraints on the iron oxide and metallic iron sextuplets: (i) the positions of the inner four peaks of each sextuplet were constrained to equal those values calculated from the positions of the outer two peaks of each sextuplet using Mössbauer spectra reported for α-Fe_2O_3 at temperatures below the Morin temperature (*31*), and those obtained from room temperature calibration spectra of metallic iron, and (ii) the peak widths and dips were constrained such that the spectral area ratio of the pairs of peaks in each sextuplet was 3/2/1. All constrained parameters were estimated on the basis of the two outermost peaks in each sextuplet since these peaks did not overlap with absorption peaks arising from iron carbide. After the central portion (the carbide portion) of the spectrum was fit reasonably well, these constraints were released. In the final fits, no constraints were imposed so that all the variables could be optimized to obtain the "best fit" of the Mössbauer spectrum.

DISCUSSION

Catalyst Deactivation via Pore-Mouth Blocking

As shown in Figs. 1 and 2, the decomposition of $Fe(CO)_5$ on nickel methanation catalysts results in significant decreases in catalyst activity within several hours. In addition, the kinetic parameters of the methanation reaction over these nickel catalysts follow a systematic trend with increasing iron content, i.e., the catalytic properties shift from those of a Ni catalyst to those of an Fe catalyst. This is evident from the data in Table 1 which presents the kinetic parameters of the Ni catalyst after exposure to various amounts of $Fe(CO)_5$ as well as those reported for Ni/Al_2O_3 and Fe/Al_2O_3 (*29*).

There are three conceivable models by which the above methanation kinetics data can be explained: (i) a monolayer model, (ii) a pore-mouth blocking model, or (iii) a combination of these two models. In the monolayer model, the Ni surface is covered with at least a monolayer of Fe. The pore-mouth blocking model postulates that the micropores in the catalyst support are blocked by the Fe particles formed during the decomposition of $Fe(CO)_5$. Reactant gas molecules are thus denied access to the Ni particles within the pores. In the combination model, the pore-mouth blocking mechanism is applicable to the micropore structure in the catalyst, while the catalytic properties of the Ni particles in the macropores are modified by Fe species deposited on the surfaces thereof. The concentrations and locations of Fe deposited on the catalyst can be determined using *in situ* Mössbauer spectroscopy. On the basis of these data, discrimination among the deactivation models can be achieved.

In situ Mössbauer spectra collected under methanation reaction conditions showed only a sharp absorption doublet to which the iron impurity in the Be windows provides a major contribution. *In situ* Mössbauer spectra obtained under H_2 treatment conditions also had a sharp absorption doublet near zero Doppler velocity. In addition, the existence of ferromagnetic iron was indicated by the presence of the two weak peaks at ca. ± 5 mm/s, which must be the outermost absorption peaks of a sextuplet. However, detailed analysis of the catalyst structure on the basis of these high temperature spectra is difficult for the following reasons. First, since the recoil-free

fraction diminishes with increasing temperature, the total spectral areas of these spectra are smaller than those of spectra collected at room temperature. Second, the Mössbauer spectra are no longer magnetically split either because the temperatures are higher than the Curie temperature or because of superparamagnetism at temperatures below the Curie temperature. Hence, in the following discussion, attention is focused on the Mössbauer spectra collected at room temperature.

Before the *in situ* Mössbauer spectra collected at room temperature are discussed, it is essential to show that the prevailing states of the catalyst at higher temperatures can be "preserved" by the quenching procedure used. Raupp and Delgass (*34*) found that only 30% of a fully carbided 10 wt% Fe/MgO catalyst was hydrogenated to metallic iron after 10 h of hydrogen treatment at 523 K. The iron carbide phase was identified as χ-carbide in a separate study (*35*). Thus, the hydrogenation of the carbide is a slow process in H_2, and the rate of hydrogenation is expected to be even slower in H_2 containing some CO, as was the case in the quenching process employed in the present study. During the quenching operation, it took only 5 min to cool the catalyst temperature to ca. 450 K. Thus, the quenching procedure used should be capable of "freezing" the catalyst states at the reaction conditions for Mössbauer spectroscopy studies. Furthermore, an examination of the catalytic methanation activities before and after quenching indicated the absence of catalyst deactivation due to the formation of $Ni(CO)_4$.

The phase diagram for Fe–Ni alloys (*36*) shows the existence of a bcc, iron-rich phase (α-phase) and of an fcc, nickel-rich phase (γ-phase). The magnetic hyperfine fields of Fe–Ni alloys with various compositions have been measured at room temperature (*37*). Hence, if an Fe–Ni alloy is formed on the Ni catalyst after $Fe(CO)_5$ treatment, its composition can be determined by comparing the measured magnetic fields (Table 2) to the reported values. The room temperature spectra (Fig. 6) collected after treatments in H_2 show broad sextuplets with hyperfine fields (324–332 kOe) essentially identical to that of bulk metallic iron (330 kOe). Thus, Fe particles free of Ni were formed during the decomposition of $Fe(CO)_5$. Furthermore, on the basis of the relative spectral areas (Table 2), these Fe particles account for a major portion of the deposited Fe. However, this does not rule out the possible existence of an Fe–Ni alloy on the $Fe(CO)_5$ treated catalyst, since this iron may behave superparamagnetically and therefore contribute to the broad singlet near zero Doppler velocity (Fe^0 "broad singlet" in Table 2). Experimental data reported elsewhere (*25*) indicate that the decomposition of $Fe(CO)_5$ on a supported Ni catalyst can indeed result in the formation of an Fe–Ni alloy.

Assuming that the recoil-free fractions of iron-containing phases in the catalyst are equal to that of the iron impurity in the Be windows, the amount of Fe deposited on the catalyst due to decomposition of $Fe(CO)_5$ can be estimated for runs NiFe-2 and NiFe-3 (where iron enriched in ^{57}Fe was used). The results of such estimates are listed in Table 4 in terms of the overall Fe/Ni ratios for these samples. Chemical analysis of the deactivated catalyst used in run NiFe-3 suggests a total Fe/Ni ratio of 10.3%, which is much higher than the 3.62% calculated from the total absorption peak area ratios. This discrepancy may result from differences in recoil-free fraction or from differences in the amount of sample being analyzed by the two techniques. In the latter respect, the iron may not be uniformly deposited through the catalyst bed, as noted in separate experiments (*25*). Thus, the Fe/Ni ratios calculated from chemical analysis and the relative areas of components in the Mössbauer spectrum are both included in Table 4. The results of chemical analysis of the used catalyst of run NiFe-1 indicate an Fe/Ni ratio of 0.84%. Since iron containing the natural

TABLE 4

Amounts of Fe-Containing Phases on Deactivated Ni Catalyst

Fe-containing phases	% Fe[a]	Fe/Ni[b]	Number of Fe Particles[b,c]
Run NiFe-2[d]		0.033	
Ferromagnetic metallic Fe	58.6		7.8×10^{14}
Fe^{2+}	11.1		—
Fe^0 (broad singlet)	30.2		—
Run NiFe-3[e]		0.036 (0.10)	
Ferromagnetic metallic Fe	64.0		9.4×10^{14} (27×10^{14})
Fe^{2+}	6.3		—
Fe^0 (broad singlet)	29.7		—

[a] Relative amounts of Fe-containing species calculated on the basis of Mössbauer spectral areas.

[b] Total amount of iron based on total Mössbauer spectral area (excluding Fe impurity in Be windows). The number in parentheses based on chemical analysis for total iron.

[c] The population of Fe particles per gram catalyst calculated assuming that all the ferromagnetic metallic iron is present as spherical particles 7 nm in diameter.

[d] After 11 h exposure to $Fe(CO)_5$.

[e] After 9.7 h exposure to $Fe(CO)_5$.

abundance of ^{57}Fe was employed in run NiFe-1, the catalyst could not be characterized using Mössbauer spectroscopy.

The ferromagnetic iron phase was identified above as being due to Fe particles free of Ni; therefore, the only Fe-containing phase which could be interacting with nickel is that which is responsible for the broad singlet in the Mössbauer spectra. From the data of Table 4 it is possible to calculate the Fe/Ni ratio for only that iron which gives rise to the broad spectral singlet. This ratio is about 1 or 3% based on Mössbauer spectroscopy or chemical analysis for total iron determination, respectively. In view of these very small Fe/Ni ratios, it would not be possible to cover the Ni surface with a monolayer of Fe unless the average Ni particle size were as large as 26–80 nm. X-Ray diffraction studies on the sintered Ni catalyst and the Fe-deactivated Ni catalyst showed no evidence for the existence of such large particles. (Actually, the average Ni particle size was so small that even the most intense diffraction peak of Ni due to (111) planes could not be distinguished from the background signal.) Thus the changes in the kinetic properties of the Ni catalyst which are induced by $Fe(CO)_5$ decomposition cannot be attributed to a covering of the Ni surface by an Fe deposit. Moreover, this monolayer model is not able to account for the decrease in catalytic activity for methanation which is observed as increasing amounts of Fe are deposited. In a separate experiment (*25*), a catalyst with its Ni surface partially covered with a uniform Fe deposit (Fe/Ni = 3.44%) showed a higher methanation activity than that of a fresh nickel catalyst.

Blockage of pore mouths by iron particles provides a plausible alternative explanation for the catalyst deactivation by the small amount of Fe deposited. This mechanistic interpretation of the data requires (i) that Fe particles (and carbon deposits associated therewith) formed at the pore entrance be of a size comparable to the diameter of the micropore structure in the Al_2O_3 support, and (ii) that the number of Fe particles formed be, at least, comparable with the number of pores in the Al_2O_3 support. An *in situ* Mössbauer spectrum collected in hydrogen at 623 K indicates that the Ni-free Fe particles (which are ferromagnetic at room temperature) are predominantly in the superparamagnetic state. The temperature at which a ferromagnetic phase behaves superparamagnetically (i.e., the blocking temperature) is a function of the particle size and the magnetic anisotropic barrier energy, K (*38, 39*). Accordingly, the average size of the metallic iron particles is estimated to be 7.0 nm, assuming values for K and the blocking temperature of 4.5×10^5 erg/cm^3 and 623 K, respectively. For the alumina support used in this study (Davison SMR-7), 23% of the pore volume is present as pores larger than 100 nm in diameter and most pores are 4.5–6.5 nm in diameter (*40*). Thus the size of the Fe particles formed via $Fe(CO)_5$ decomposition is indeed comparable to the diameter of the micropore structure of the Al_2O_3 support used. The conversion of these Fe particles into χ-carbide

under methanation reaction conditions has no effect on this argument. On the basis of the published crystallographic parameters of χ-carbide (*41*) and the density of bulk metallic iron, the increase in particle size upon conversion of metallic iron to χ-carbide is ca. 4%. Any carbon deposition on the iron, however, would increase the effective diameter of the iron particles.

The γ-Al_2O_3 support has a specific surface area of 260 m^2/g and a pore volume of about 1 cm^3/g (*40*). If one assumes that the average pore length is one-third the radius of the support (*42*), then the number of average-size pores in the γ-Al_2O_3 can be estimated to be about 4×10^{14} per gram of catalyst. The number of Fe particles in the deactivated catalyst can also be calculated, if the Fe particles are assumed to be uniform in size, i.e., spherical particles 7 nm in diameter. These are listed in the last column of Table 4. These semiquantitative calculations suggest that there are indeed enough Fe particles to block a substantial fraction of the micropores of the supported catalyst.

Carlton and Oxley (*43*) studied the kinetics of heterogeneous decomposition of $Fe(CO)_5$ on a heated filament. They found that at temperatures higher than 470 K the rate of decomposition was controlled by the diffusion of $Fe(CO)_5$ from the bulk gas phase to the gas–solid interface. At 620–650 K, the decomposition temperatures employed in the present study, it may be anticipated that the rate of $Fe(CO)_5$ decomposition is severely limited by diffusion within the pores of the support. It has been reported that the decomposition of $Ni(CO)_4$ is diffusion-controlled in the same γ-Al_2O_3 support at similar temperatures (*8*). This is why most of the $Fe(CO)_5$ would decompose at the pore mouths, forming Fe particles of a size comparable to the diameter of the micropores.

Direct evidence for the preferential decomposition of iron near the pore mouths of the alumina support is contained in the Mössbauer spectra. It has been shown in the literature (*30, 44*) that iron on alumina at loadings less than ca. 1 wt% cannot be reduced to the metallic state. Instead, Fe^{2+} is stabilized by interaction with the support. As shown in Table 2, however, the contribution of Fe^{2+} is of minor importance in the Mössbauer spectra of the iron-containing Ni catalyst. Since the average Fe loading in the catalyst is ca. 0.2–0.5 wt%, the absence of a significant spectral signal from Fe^{2+} indicates that the local concentration of iron must be significantly higher than the average concentration. This high local concentration of iron is present at the most accessible surfaces of the alumina support, i.e., at the pore mouths.

It will be shown in the subsequent paper (*25*) that pore-mouth blocking by iron deposits is substantiated by BET surface area measurements on alumina powder exposed to iron carbonyl under methanation reaction conditions (sample AlFe-1). When compared to iron-free alumina, the iron-deposited sample had a lower BET surface area. In addition, the rate of nitrogen adsorption was slower for the iron-containing sample, as would be expected due to pore-mouth blocking. However, as discussed in detail elsewhere (*25*), the observed decrease in the activation energy for methanation upon incorporation of Fe into Ni/Al_2O_3 catalysts cannot be attributed to diffusion limited kinetics since the reaction rate dependence on the CO pressure remained essentially unchanged with increasing amounts of iron deposited.

Finally, it may be suggested that the high concentration of iron at the pore mouths of the iron-deactivated nickel methanation catalysts may induce a shift in catalyst selectivity. For example, the observed decrease in methanation activity of the iron-deposited catalysts could be attributed to a change in selectivity from CH_4 to higher hydrocarbons. However, due to the high H_2/CO ratios (ca. 7 : 1) and reaction temperatures (ca. 620–650 K) used in this study, no hydrocarbons higher than CH_4 could be detected in the reactor effluent. Thus, the pri-

mary effect of iron deposited on Ni/Al_2O_3 catalysts during iron carbonyl decomposition under methanation reaction conditions is catalyst deactivation and not a change in catalyst selectivity.

Iron Carbide Formed at Methanation Conditions

The formation of carbides on supported and unsupported iron catalysts under Fischer–Tropsch synthesis conditions has been extensively studied (*15, 35, 45–53*). The formation of a specific carbide phase depends on particle size, support, and synthesis conditions. ε'-Carbide ($Fe_{2.2}C$) has been observed on silica-supported catalysts (*15, 35, 46*). ε-Carbide (Fe_2C) has been detected on silica-supported catalysts (*15, 35*), on promoted, fused iron catalysts (*48, 49, 51*), and unpromoted, unsupported iron catalysts (*47, 52*). The formation of χ-carbide (Fe_5C_2) has been noted on promoted, fused iron catalysts (*49, 50*) and on various supported catalysts (*35*). Mössbauer spectroscopy is a powerful tool in identifying iron carbide phase(s) which show magnetic hyperfine splitting, since Mössbauer spectra of various carbide phases are characterized not only by the magnetic fields but also by the number of magnetically split sextuplets (*15, 35*). However, the reported Mössbauer parameters for superparamagnetic ε'- and ε-carbides (i.e., for particles smaller than ca. 10 nm in size (*47*)) are similar to each other (*46–48*). Thus, the unambiguous identification of iron carbide phase(s) in the superparamagnetic state is difficult.

The solid state properties of supported Fe–Ni alloy catalysts after Fischer–Tropsch synthesis at atmospheric pressures have recently been characterized using Mössbauer spectroscopy (*15, 35, 45, 53*). Raupp and Delgass (*35, 53*) found that no bulk carbides were formed on a 5% Fe–5% Ni/SiO_2 catalyst at synthesis conditions. Their particle size was sufficiently small (ca. 4.0 nm) that the room temperature spectrum showed a broad superparamagnetic singlet characteristic of an Fe–Ni alloy. Formation of a carbide phase was noted only on a phase-separated catalyst. On the other hand, Unmuth *et al.* (*15, 45*) reported the formation of ε- or ε'-carbide on a 4% Fe–1% Ni/SiO_2 catalyst (with particles ca. 10 nm in size) after temperature-programmed reaction in a $3H_2$: CO reaction mixture. Mössbauer spectra of the reduced catalyst indicated the existence of both an iron-rich bcc phase and a nickel-rich fcc phase. Thus, the different catalyst states at similar reaction conditions may be attributed to the different Fe–Ni phases and perhaps the different particle sizes on the catalysts used. Indeed, Amelse *et al.* (*54*) noted that on Fe–Ni catalysts (with ca. 20 nm particles), the iron-rich bcc phase was more easily carbided than the nickel-rich fcc phase.

The Mössbauer spectra collected in the present study under reaction conditions showed an asymmetric doublet. The scarcity of published Mössbauer spectra for iron carbides at elevated temperatures and the similarity of Mössbauer spectra for superparamagnetic iron carbides discussed above make the identification of the carbide phase impossible at high temperatures. The room temperature spectra following quenching from reaction conditions (Fig. 5) show partially collapsed sextuplets due to small iron carbide particles. This superparamagnetism also makes it difficult to identify the carbide phase by determining its Curie temperature, as done by Raupp and Delgass (*35*), and Loktev *et al.* (*51*). Thus, identification of the carbide phase was carried out at 10 K in the liquid helium refrigerator. The carbide portion of the spectrum (Fig. 7) was fitted with three sextuplets. As seen in Table 3, the computer-fitted magnetic hyperfine fields of the three sextuplets agree very well with published data for χ-carbide at 4 K (*33*). Moreover, the relative populations of iron atoms in the three magnetically different sites, as calculated from the relative spectral areas, is 2/1.9/0.6, which again agrees with the litera-

ture values for χ-carbide, i.e., 2/2/1 (*55*). Thus, it is concluded that the stable carbide phase under methanation reaction conditions is the χ-carbide.

In addition to the carbide phase, the low temperature Mössbauer spectrum (Fig. 7) indicates the presence of two more ferromagnetic iron-containing phases. Their magnetic hyperfine fields, 338 and 452 kOe (see Table 3), are too large to be due to any carbide phase or Ni-rich Fe–Ni alloy (*37*). Instead, the computer-fitted magnetic field of 338 kOe is equal to the reported value for bulk metallic iron at ca. 4 K (*32*). This metallic iron is most likely located in the core of the iron particles formed by the decomposition of $Fe(CO)_5$. This conclusion is based on the observation that complete carburization of a 10% Fe/SiO_2 catalyst (particle size 7.5 nm) required a 3-h treatment in synthesis gas ($H_2/CO = 3.3$) at 523 K (*34*) while the catalyst sample of the present study received only a 25-min treatment in synthesis gas ($H_2 : CO = 8 : 1$) at 648 K before the low temperature Mössbauer spectroscopy characterization. The third ferromagnetic phase in the spectrum is characterized by a magnetic field of 452 kOe, which is much larger than the fields due to either metallic iron or iron carbides. This phase must be an iron oxide, although the observed magnetic field is much smaller than the literature value for α-Fe_2O_3 (ca. 540 kOe at temperatures near absolute zero (*31*)). Niemantsverdriet *et al.* (*52*) also noted the presence of an iron oxide phase with a reduced magnetic field (H = 500 kOe) on their catalyst sample at 4.2 K which was not detected at 77 K. Assuming that the oxide phase exists as a shell of uniform thickness on the Fe particles, its thickness has been estimated at 0.3 nm using the relative spectral area and the above determined average particle size of 7.0 nm. In addition, the magnetic character of this thin-shell iron oxide may be different from that of a bulk oxide, leading to a smaller magnetic field. Due to the sample transfer procedure used, it is difficult to determine the origin of this oxide phase. It may be formed either during the sample transfer process or under methanation conditions.

Although the results reported elsewhere (*25*) indicate that Fe–Ni interactions may exist on the Fe-deactivated Ni catalyst, the low temperature spectrum (Fig. 7) can be adequately fitted with only the three Ni-free components discussed above. It is thus suggested that any Fe–Ni alloy particles present after reduction were carbided under methanation reaction conditions. Indeed, Unmuth *et al.* (*15*) have suggested that both the iron-rich and nickel-rich Fe–Ni alloys could be carbided under reaction conditions.

The room temperature spectra following quenching from reaction conditions (Fig. 5) are, in fact, similar to those reported by Unmuth *et al.* (*15*). Furthermore, the apparent magnetic fields of spectra (c) and (d) (determined from the separation between the two outermost observable absorption peaks) are estimated to be between 180 and 195 kOe, which are comparable to the values of 183 to 185 kOe reported for the two outermost peaks in their spectra (*15*). However, the liquid helium temperature Mössbauer spectrum of the present study indicates that the carbide phase is a χ-carbide, rather than the ε'- or ε-carbide suggested by Unmuth *et al.* In addition, the low temperature study also indicated the presence of two more ferromagnetic phases which were not detected in the room temperature studies, although the origin of the oxide phase is uncertain.

CONCLUSIONS

The incorporation of Fe into alumina-supported nickel catalysts via the decomposition of iron carbonyl results in significant catalyst deactivation for the methanation reaction. In addition, the reaction kinetics parameters are shifted from those of a nickel catalyst toward those of an iron catalyst as the amount of Fe deposition increases. The observed catalyst deactivation is due primarily to pore-mouth

blocking by Fe particles. These Fe particles, formed during the diffusion-limited decomposition of $Fe(CO)_5$, effectively block the access of reactants to the micropore structure in the high surface area support. Consequently, the effective Ni surface area and the catalyst activity associated therewith are reduced. As a result of this decrease in effective Ni surface area and the increase in Fe surface area, the kinetic behavior of the iron-deactivated nickel catalyst is shifted toward that of iron. While it is tempting to interpret the sole role of iron in altering the kinetics of methanation over Ni/Al_2O_3 to pore-mouth blocking, it will be shown in a subsequent paper (*25*) that iron may also interact with nickel particles in the macropores of the alumina support. This Fe–Ni interaction may contribute to the shifts in the kinetic properties of Fe deactivated Ni catalysts. Finally, the state of the Fe deposit under methanation reaction conditions has been identified as a χ-carbide using Mössbauer spectroscopy at liquid helium temperature.

ACKNOWLEDGMENTS

We thank Mr. G. L. Vogler for his technical assistance during this study. Financial support from Department of Energy (ET-78-G-01-3380) is also gratefully acknowledged. Finally, we thank Professor C. H. Bartholomew (Brigham Young University) for stimulating discussions during the early stages of this work.

REFERENCES

1. Satterfield, C. N., "Heterogeneous Catalysis in Practice." McGraw-Hill, New York, 1980.
2. Woodward, C., *Hydrocarbon Process.* **56**(1), 136 (1977).
3. Rao, M. J., Ramacharyulu, M., and Vaidyeswaran, R., *Chem. Ind. Dev.* **11,** 15 (1977).
4. Hausberger, A. L., Knight, C. B., and Atwood, K., *Adv. Chem. Ser.* **146,** 47 (1975).
5. Kuo, H. K., Ganesan, P., and De Angelis, R. J., *J. Catal.* **64,** 303 (1980).
6. Richardson, J. T., and Crump, J. G., *J. Catal.* **57,** 417 (1979).
7. Williams, A., Butler, G. A., and Hammonds, J., *J. Catal.* **24,** 352 (1972).
8. Shen, W. M., Dumesic, J. A., and Hill, C. G., Jr., *J. Catal.* **68,** 152 (1981).
9. Rostrup-Nielsen, J. R., and Pedersen, K., *J. Catal.* **59,** 395 (1979).
10. Wentrcek, P. W., McCarty, J. G., Ablow, C. M., and Wise, H., *J. Catal.* **61,** 232 (1980).
11. Pannell, R. B., Chung, K. S., and Bartholomew, C. H., *J. Catal.* **46,** 340 (1977).
12. Ng, C. F., and Martin, G. A., *J. Catal.* **54,** 384 (1978).
13. Mills, G. A., and Steffgen, F. W., *Catal. Rev.–Sci. Eng.* **8,** 159 (1973).
14. Gardner, D. C., and Bartholomew, C. H., *Ind. Eng. Chem. Prod. Res. Dev.* **20,** 80 (1981).
15. Unmuth, E. E., Schwartz, L. H., and Butt, J. B., *J. Catal.* **63,** 404 (1980).
16. Bartholomew, C. H., Weatherbee, G. D., and Jarvi, G. A., *Chem. Eng. Commun.* **5,** 125 (1980).
17. Dalla Betta, R. A., Piken, A. G., and Shelef, M., *J. Catal.* **40,** 173 (1975).
18. Wentrcek, P. R., McCarty, J. G., Wood, B. J., and Wise, H., *Amer. Chem. Soc. Div. Fuel Chem. Prepr.* **21,** 52 (1976).
19. Goodman, D. W., Kelley, R. D., Madey, T. E., and Yates, J. T., Jr., *J. Catal.* **63,** 236 (1980).
20. McCarty, J. G., and Madix, R. J., *Surf. Sci.* **54,** 121 (1976).
21. Trimm, D. L., *Catal. Rev.–Sci. Eng.* **16,** 155 (1977).
22. Bartholomew, C. H., *Catal. Rev.–Sci. Eng.* **24,** 67 (1982).
23. Tart, K. R., and Rampling, T. W. A., *Hydrocarbon Process.* **60**(4), 114 (1981).
24. Haynes, W. P., Forney, A. J., Elliott, J. J., and Pennline, H. W., *Adv. Chem. Ser.* **146,** 87 (1975).
25. Shen, W. M., and Dumesic, J. A., *J. Catal.* **84,** 135 (1983).
26. Shen, W. M., Dumesic, J. A., and Hill, C. G., Jr., *Rev. Sci. Instrum.* **52,** 858 (1981).
27. Sørensen, K., Internal Report No. 1, Laboratory of Applied Physics II, Technical University of Denmark, Lyngby, Denmark, 1972.
28. Shen, W. M., Ph.D. thesis, Department of Chemical Engineering, University of Wisconsin-Madison, 1982.
29. Vannice, M. A., *J. Catal.* **37,** 449 (1975).
30. Dumesic, J. A., and Topsøe, H., *Adv. Catal.* **26,** 121 (1977).
31. Greenwood, N. N., and Gibb, T. C., "Mössbauer Spectroscopy." Chapman & Hall, London, 1971.
32. Preston, R. S., Hanna, S. S., and Herberle, J., *Phys. Rev.* **128,** 2207 (1962).
33. Le Caer, G., Dubois, J. M., and Senateur, J. P., *J. Solid State Chem.* **19,** 19 (1976).
34. Raupp, G. B., and Delgass, W. N., *J. Catal.* **58,** 361 (1979).
35. Raupp, G. B., and Delgass, W. N., *J. Catal.* **58,** 348 (1979).
36. Hansen, M., "Constitution of Binary Alloys." McGraw-Hill, New York, 1958.
37. Johnson, C. E., Ridout, M. S., and Cranshaw, T. E., *Proc. Phys. Soc. (London)* **81,** 1079 (1963).

38. Mørup, S., Topsøe, H., and Lipka, J., *J. Phys.* **37,** C-287 (1976).
39. Mørup, S., and Topsøe, H., *Appl. Phys.* **11,** 63 (1976).
40. Physical properties provided by manufacturer.
41. Powder Diffraction File 20-508, JCPDS, International Center for Diffraction Data, Swarthmore, Pa.
42. Hill, C. G., Jr., "An Introduction to Chemical Engineering Kinetics and Reactor Design." Wiley, New York, 1977.
43. Carlton, H. E., and Oxley, J. H., *AIChE J.* **11,** 79 (1965).
44. Topsøe, H., Dumesic, J. A., and Mørup, S., *in* "Applications of Mössbauer Spectroscopy" (R. L. Cohen, Ed.), Vol. 2, p. 55. Academic Press, New York, 1980.
45. Unmuth, E. E., Schwartz, L. H., and Butt, J. B., *J. Catal.* **61,** 242 (1980).
46. Amelse, J. A., Butt, J. B., and Schwartz, L. H., *J. Phys. Chem.* **82,** 558 (1978).
47. Le Caer, G., Simon, A., Lorenzo, A., and Génin, J. M., *Phys. Status Solidi A* **6,** K97 (1971).
48. Maksimov, Yu. V., Suzdalev, I. P., Arents, R. A., and Loktev, S. M., *Kinet. Katal.* **15,** 1293 (1974).
49. Hofer, L. J. E., Cohn, E. M., and Peebles, W. C., *J. Amer. Chem. Soc.* **71,** 189 (1949).
50. Maksimov, Yu. V., Suzdalev, I. P., Arents, R. A., Goncharov, I. V., Krautsov, A. V., and Loktev, S. M., *Kinet. Katal.* **13,** 1600 (1972).
51. Loktev, S. M., Makarenkova, L. I., Slivinskii, E. V., and Entin, S. D., *Kinet. Katal.* **13,** 1042 (1972).
52. Niemantsverdriet, J. W., van der Kraan, A. M., van Dijk, W. L., and van der Baan, H. S., *J. Phys. Chem.* **84,** 3363 (1980).
53. Raupp, G. B., and Delgass, W. N., *J. Catal.* **58,** 337 (1979).
54. Amelse, J. A., Schwartz, L. H., and Butt, J. B., *J. Catal.* **72,** 95 (1981).
55. Bernas, H., Campbell, I. A., and Fruchart, R., *J. Phys. Chem. Solids* **28,** 17 (1967).